

μ TRISTAN

Yu Hamada¹, Ryuichiro Kitano^{1,3}, Ryutaro Matsudo¹, Hiromasa Takaura¹
and Mitsuhiro Yoshida^{2,3}

¹*KEK Theory Center, Tsukuba 305-0801, Japan*

²*KEK Accelerator department, Tsukuba 305-0801, Japan*

³*Graduate University for Advanced Studies (Sokendai), Tsukuba 305-0801, Japan*

Abstract

The ultra-cold muon technology developed for the muon $g - 2$ experiment at J-PARC provides a low emittance μ^+ beam which can be accelerated and used for realistic collider experiments. We consider the possibility of new collider experiments by accelerating the μ^+ beam up to 1 TeV. Allowing the μ^+ beam to collide with a high intensity e^- beam at the TRISTAN energy, $E_{e^-} = 30$ GeV, in the storage ring with the same size as TRISTAN (the circumference of 3 km), one can realize a collider experiment with the center-of-mass energy $\sqrt{s} = 346$ GeV, which allows productions of the Higgs bosons through the vector boson fusion processes. We estimate the deliverable luminosity with existing accelerator technologies to be at the level of $5 \times 10^{33} \text{ cm}^{-2} \text{ s}^{-1}$, with which the collider can be a good Higgs boson factory. The $\mu^+\mu^+$ colliders up to $\sqrt{s} = 2$ TeV are also possible by using the same storage ring. They have a capability of producing the superpartner of the muon up to TeV masses.

1 Introduction

It is important to perform measurements of the Higgs boson properties in order to uncover the mysteries of the electroweak symmetry breaking. Measurements of the couplings at the level of a percent probe the energy scale of more than a TeV, where some hints for the origin of our peculiar vacuum are expected to be hidden. This motivates us to consider high energy lepton colliders that copiously produce Higgs bosons. The e^+e^- linear colliders such as ILC [1] and CLIC [2] can indeed make such measurements possible. The lowest energy option of the ILC, $\sqrt{s} = 250$ GeV, will give a great improvement in the knowledge of fundamental physics.

The $\mu^+\mu^-$ colliders have also been considered as a future possibility, where less synchrotron radiation than the case of the electron enables us to consider a few kilometer-level circular colliders with TeV energies (see e.g., Ref. [3, 4]). Not only Higgs boson physics, a direct probe of new physics will be possible with such high-energy colliders. (See Ref. [5] for a recent summary.)

There have been studies of Higgs boson physics at high-energy muon colliders. Since the cross sections of the vector boson fusion processes are enhanced at high energies, very precise measurements of Higgs couplings have been demonstrated to be possible [6, 7]. Those studies, however, assume luminosities which demand further developments of muon cooling and accelerating technologies [8].

In this paper, we instead consider μ^+e^- and $\mu^+\mu^+$ colliders, which can deliver good enough luminosities for physics researches within the existing technologies. While a narrow μ^- beam for muon colliders has not been achieved yet, there is an established technology to create a low-emittance μ^+ beam by using the ultra-cold muons [9]. At the μ^+e^- collider, the Higgs bosons are produced via the WW/ZZ fusion as in the case of the $\mu^+\mu^-$ or e^+e^- colliders while background events through the s -channel annihilation, such as W^+W^- and $q\bar{q}$ final states, are absent. Using the storage ring with the circumference of about 3 km as a reference design, we consider a collider with the center-of-mass energy, $\sqrt{s} = 346$ GeV, by accelerating the electrons and the muons to 30 GeV and 1 TeV, respectively. Using the same tunnel, it is possible to simultaneously build a $\mu^+\mu^+$ collider with $\sqrt{s} = 2$ TeV, which can directly reach TeV physics.

In Refs. [10, 11], good physics performances of μ^+e^- colliders have been demonstrated for the measurements of the Higgs boson couplings as well as searches for lepton flavor violating interactions by assuming integrated luminosities of the order of ab^{-1} . It is then an important question whether such a collider can be constructed in a timely manner.

Two independent projects at KEK have achieved important accomplishments which actually enable us to plan the construction of high energy μ^+e^- and $\mu^+\mu^+$ colliders now. One is the world's highest luminosity at the SuperKEKB experiment, which aims for the instantaneous luminosity of $8 \times 10^{35} \text{ cm}^{-2} \text{ s}^{-1}$ [12]. An upgrade to have a polarized e^- beam is under consideration [13] that will be important for the Higgs factory. Another important technology is the production of the ultra-cold muons, which is developed for the precise measurements of the $g - 2$ of the muon at J-PARC [14]. The positive muons from the pion decay are stopped at a surface of a material and trap electrons to form muoniums. By shooting a laser to strip electrons, one can obtain ultra-cold positive muons, that can be accelerated to be used for a low-emittance beam for colliders.

Both technologies are already well studied. Considering a similar proton driver to that in J-PARC and using all of the protons for muon production, the production rate of the ultra-cold positive muons is estimated to be at the level of 10^{13-14} muons per second. The ultra-cold technology provides the normalized emittance of the μ^+ beam to be of 4 mm mrad [14]. By accelerating the μ^+ beam up to TeV and focusing it at the interaction point, the beam size is reduced to a few μm . When we make the μ^+ beam collide with the intense e^- beam at the TRISTAN energy, 30 GeV, our estimate of the instantaneous luminosity is of the order of $5 \times 10^{33} \text{ cm}^{-2} \text{ s}^{-1}$ per detector, which is at the same level as the design of the ILC. By assuming ten years of running with a single detector, the integrated luminosity can be as high as 1 ab^{-1} , with which 0.1 million Higgs bosons are produced through the W boson fusion process.

A larger storage ring such as the size of the Tevatron allows higher energy colliders. By assuming that the dipole magnets at about 16 T is available by the time of the construction, one can reach $\sqrt{s} = 775 \text{ GeV}$ with 50 GeV electrons and 3 TeV muons. The possible luminosity is estimated to be similar to the case of the 1 TeV muons by assuming the same beam power. Since the production cross section via the W boson fusion process is enhanced at high energies, 0.5 million Higgs bosons can be produced with the same luminosity, 1 ab^{-1} . The pair production of Higgs bosons is also enhanced to be $O(100)$ events, with which one can expect the measurement of the self-coupling of the Higgs boson.

One can also consider a $\mu^+\mu^+$ collider [15] with $\sqrt{s} = 2 \text{ TeV}$ at the 3 km ring or 6 TeV for the large ring option. The instantaneous luminosity is estimated to be of the order of $6 \times 10^{32} \text{ cm}^{-2} \text{ s}^{-1}$ by assuming the same μ^+ beam as above. Although the Higgs production is possible through the Z boson fusion process, the number of the events is much fewer than the μ^+e^- colliders due to the limited luminosity and the small Z boson fusion cross sections.

On the other hand, the $\mu^+\mu^+$ colliders have a good reach for new particle searches, such as the pair production of the superpartners of the muon.

The high intensity μ^+ facility for the μ^+e^- or $\mu^+\mu^+$ colliders will provide rich physics opportunities such as precision muon physics, muon engineering, material science as well as neutrino physics. One can also expect future developments towards the $\mu^+\mu^-$ colliders or even possibly neutrino colliders. Starting with a μ^+e^- collider may be a good strategic option for future particle physics.

This paper is organized as follows. In the next section, we discuss the design of the accelerator complex, and estimate the possible instantaneous luminosity of the μ^+e^- and $\mu^+\mu^+$ colliders. The Higgs boson productions at the colliders are studied in Section 3 by using the estimated luminosity, and the case with the larger ring option is studied in Section 4. We briefly discuss the requirements for the detectors in Section 5 in order for the Higgs coupling measurements to be possible. The reaches of the superparticle searches at μ^+e^- and $\mu^+\mu^+$ colliders are estimated in Section 6. Section 7 is devoted to the summary.

2 Ultra-cold muons and μ^+ accelerator

We discuss the conceptual design of the μ^+ accelerator and the storage ring. We show the rough sketch in Fig. 1. Based on this design, we estimate the possible instantaneous luminosity of the μ^+e^- and $\mu^+\mu^+$ colliders. The design is based on the muon production and re-acceleration experiments at the J-PARC Materials and Life Science Experimental Facility (MLF) but we extended the part of the pion production target and the pion stopping target so that the proton beam is efficiently used for the production of ultra-cold muons. For the technology of the re-acceleration of the ultra-cold muons, see Ref. [9]. The studies of the muon collider [3] are taken as a reference for the design concept of the muon acceleration and storage.

2.1 Proton accelerator and pion production ring

The first stage of the μ^+ production is to deliver an intense proton beam to the pion production target. We assume the beam parameters of the proton LINAC (Linear Accelerator) and RCS (Rapid-Cycling Synchrotron) to be similar to those in J-PARC with the beam power of 2 MW. The 2-bunch proton beam with the bunch charge $6.6 \mu\text{C}$ ($= 4.1 \times 10^{13}$ protons) is accelerated to 3 GeV with the repetition rate of 50 Hz. The operation at 50 Hz is set by the

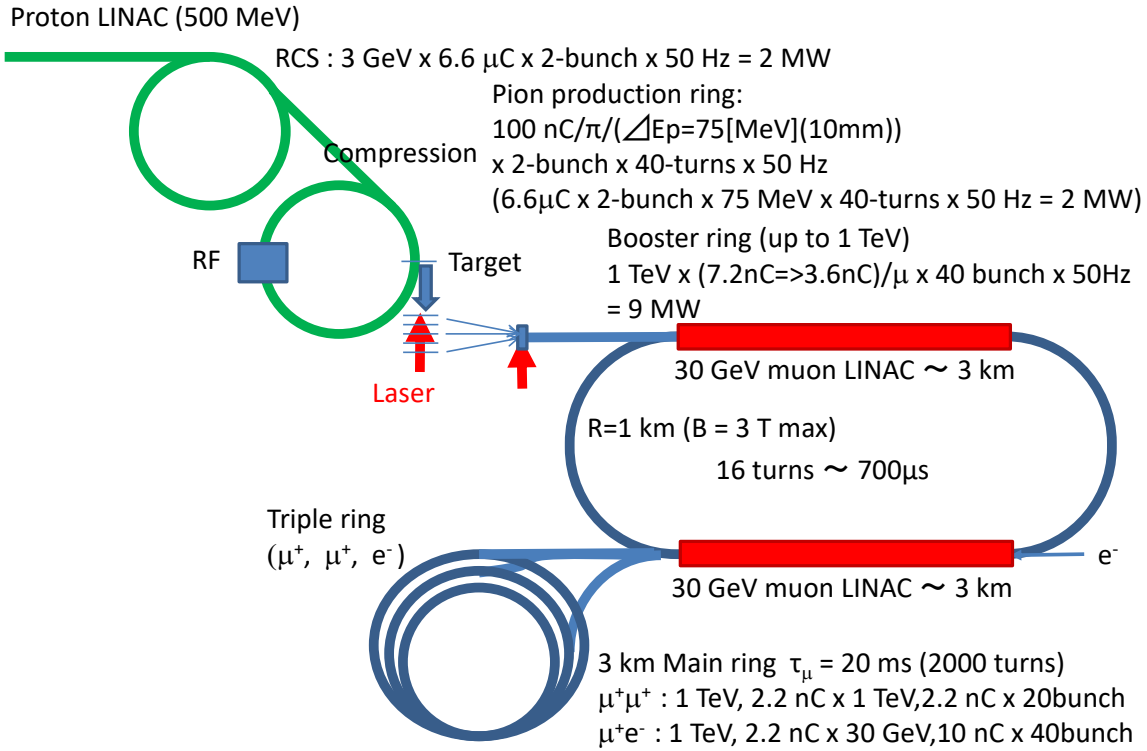


Figure 1: Conceptual design of the $\mu^+e^-/\mu^+\mu^+$ collider

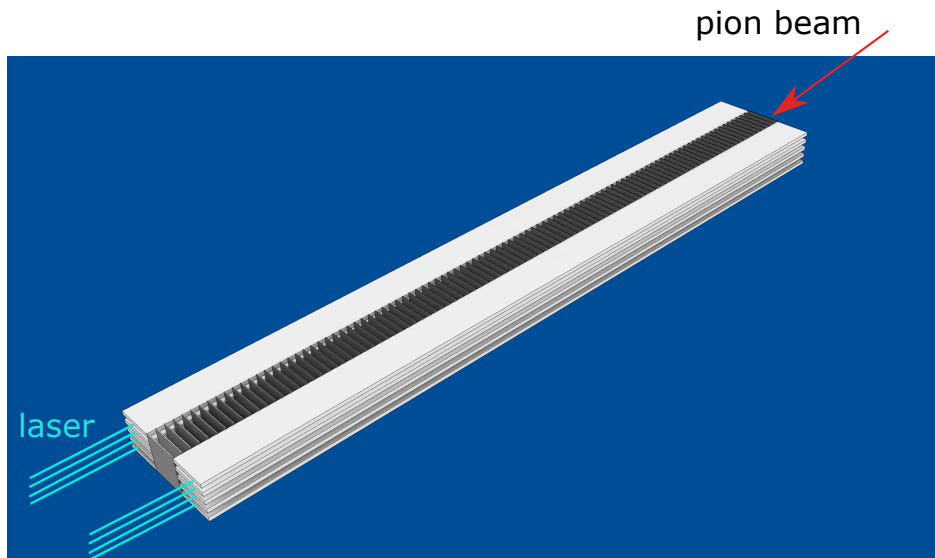


Figure 2: The pion stopping target surrounded by silica aerogel for muonium production and laser ionization.

lifetime of the muon at the energy of 1 TeV, $\gamma\tau_\mu = 20$ ms, so that a new beam is injected after muons spend their lifetime in the storage ring.

The 3 GeV proton beam is transported to the pion production ring, where the graphite target with the thickness of 10 mm is placed. The proton beam is recirculated to repeatedly hit (40 times for each bunch) the target. Such a configuration is possible by using the longitudinal phase rotation with suitable R_{56} and the RF cavity to compensate the decreased energy by the graphite target inside the ring. The energy loss of each proton by the collision is estimated to be 75 MeV (2.5 % energy loss), which amounts to 2 MW power consumption used for the recovery of the beam energy.

The cross section of the pion production process, $p + C \rightarrow \pi + X$, is 150 mb at the proton energy of 3 GeV. The number of generated pions is calculated as 0.016/proton for the target thickness of 10 mm. It results in the pion charge of 110 nC/bunch (times 40 turns times 2 bunches) at the rate of 50 Hz.*

The produced charged pions mostly travel to the beam direction and are transported to the large facility of the multi-layer pion stopping target (Fig. 2) which we explain in the next subsection. This part is different from the J-PARC configuration, where only the pions stopping at the production target, which are actually a small part of the produced pions, are used for the muon production. Instead, we use the majority of the produced pions, which do not stop at the graphite target. We estimate the efficiency of the transportation to the stopping target as 50 % considering the pion lifetime and the pion loss by interactions with materials.

2.2 Surface muon production and cooling

The multi-layered tungsten foil target is used to stop the generated pion beams. In order to completely stop the pions, we need a thousand layers of 1 mm foils placed with the interval of 1 cm [16]. This requires a large target system such as 10 m length in total. The intervals are necessary to extract surface muons from the decay of the stopped pions. A conceptual design is shown in Fig. 2. Positively charged surface muons (μ^+) are transported to the multiple layered silica aerogel target (placed just next to the tungsten foils), where the muons capture electrons to form muoniums (the μ^+e^- bound state). The aerogel target needs to have a

*The proton beam reduces its bunch charge as it hits the graphite target, since some of the protons turn into pions. As a result, the 40 pion bunches do not have the same charge. In the present study we neglect the reduction of the pion charge for simplicity. A detailed study of the proton loss and the pion loss is left for a future work. We remark, however, that it is possible to realize the pion number (or the muon number) given here simply by raising the initial proton beam power.

length of 10 m with a layer structure in the vertical direction so that one can shoot lasers in the gaps. The neutral muonium atoms are thermally diffused from the aerogel and ionized by the Lyman- α laser. The ionized μ^+ has a very small momentum spread, which is called the ultra-cold muon.

The efficiency for the production of the ultra-cold muons in total is estimated to be 14 % from the following estimated efficiencies: 52 % for the muonium formation, 60 % for the vacuum yield, 60 % after the loss of muoniums due to the decay, and 73 % for the laser ionization[†].

The ultra-cold muons spread over 10 m are in turn collected and transported to the second aerogel target with the size of a few cm. There, the muonium is formed again and re-ionized by laser. The two bunches of muons from the pion production ring are combined at the second muon target by tuning the timing of the laser irradiation. The efficiency to produce the ultra-cold muons at the second muon target is assumed as 50 %. Such high efficiency should be possible since a very thin target is used for the uniform muon energy. In total, the efficiency to obtain the ultra-cold muons from the stopped pions is 6.8 %.

Combining with the 50 % efficiency of the pion stopping and the pion production rate of 0.016/proton in the previous subsection, we obtain the number of the ultra-cold muons as 5.5×10^{-4} /proton. This amounts to 7.2 nC ultra-cold muons/bunch by combining two bunches of 6.6 μC protons. By taking into account 40 turns of the proton beam in the production ring at the 50 Hz operation, we have 9.0×10^{13} muons/s.

Compared with the J-PARC MLF experiments, the number of muons is enhanced by $O(10^5)$. This is basically due to the improvement in the efficiency to collect pions and muons. The efficiency at J-PARC MLF is much less than the ideal situation as it is designed mainly for the neutron production in the downstream. In the condition of the J-PARC MLF, the number of stopped pions in the graphite target of 20 mm length is 1.5×10^{-3} /proton. Among them, those which stopped in the region of the thin surface of 0.5 mm can be used as the surface muons, whose number is 3×10^{-5} /proton. The solid angle to cover the muon capture is 108 mSr, that reduces the number to 3×10^{-7} /proton, and 1/3 of them can be transported to the experimental site. In total, the number of muons which can be used in the experiment is 1×10^{-7} /proton. Comparing with our design, 5.5×10^{-4} /proton, and 40 turns times 2 bunches of proton beams, one can see the enhancement of $O(10^5)$.

[†]We thank Cedric Zhang to provide us with those numbers.

2.3 Muon accelerator

The ultra-cold muons are pre-accelerated and injected to the booster ring of the race-track shape (see Fig. 1). The length of the LINAC part is 3 km and there are arc sections with $R = 1$ km where the alternative gradient bending magnet of 3 T is used. The booster ring is used to accelerate the μ^+ beam up to the energy of 1 TeV. In each of the two LINAC parts of the booster ring, the μ^+ beam is accelerated by 30 GeV, with which 1 TeV beam is achieved by 16 turns. This takes about 700 μ s. The LINAC is also used for the electron acceleration intermittently for the μ^+e^- collider.

During the acceleration, about a half of the muons decays and the bunch charge is reduced to about 3.6 nC. Taking into account the beam loss, the total beam loading is about 9 MW.

2.4 Main ring and the luminosity

The accelerated beam is transported to the main ring with the circumference of 3 km. In accordance with the injection rate at 50 Hz, we keep the muon beam in the main ring for 20 ms, which is equal to the muon lifetime. Due to the decay of the muons during this time, the time-average number of the muons is $(1 - 1/e)N_{\text{initial}}$ with $N_{\text{initial}} = 3.6$ nC, which reduces to about 2.3 nC. In general, for an injection rate at $50/\kappa$ Hz, the reduction factor of the time-average number is given by $(1 - e^{-\kappa})/\kappa$. A large κ reduces the luminosity linearly while a small κ requires more electric power consumption at the booster ring. We take $\kappa = 1$ as the optimal choice.

For the $\mu^+\mu^+$ collider, the μ^+ beam is split into two beams, so that each beam has 20 bunches, while the μ^+e^- collider can use all the 40 bunches. The collision frequency, f_{rep} , for the 3 km ring is 100 kHz times the number of bunches, i.e.,

$$f_{\text{rep}}^{(\mu^+e^-)} = 4 \text{ MHz}, \quad f_{\text{rep}}^{(\mu^+\mu^+)} = 2 \text{ MHz}, \quad (1)$$

respectively.

By the ultra-cold muon technology, one can obtain the normalized emittance, $\beta\gamma\epsilon$, of the μ^+ beam to be 4 mm mrad [14]. By the acceleration up to 1 TeV, i.e., $\beta\gamma \sim 10^4$, the emittance is reduced to $\epsilon = 420$ nm mrad. By taking the realistic values of the beta functions of the collision point as $\beta_x = 30$ mm and $\beta_y = 7$ mm, we obtain the beam sizes σ_x and σ_y as

$$\sigma_x = 3.6 \text{ } \mu\text{m}, \quad \sigma_y = 1.7 \text{ } \mu\text{m}. \quad (2)$$

We conservatively assume the same focusing of the e^- beam although much better focusing should be possible by comparing with the design of SuperKEKB.

The number of muons is reduced at the collision point by the decay of μ^+ in the storage ring as stated above. By taking 2.3 nC as the bunch charge, the number of μ^+ per bunch as

$$N_{\mu^+} = 1.4 \times 10^{10}. \quad (3)$$

For the e^- beam, we take 10 nC as a realistic bunch charge, i.e.,

$$N_{e^-} = 6.2 \times 10^{10}. \quad (4)$$

By using the formula for the instantaneous luminosity,

$$\mathcal{L} = \frac{N_{\text{beam1}} N_{\text{beam2}}}{4\pi\sigma_x\sigma_y} f_{\text{rep}}, \quad (5)$$

we obtain the luminosity of the μ^+e^- collider as

$$\mathcal{L}_{\mu^+e^-} = 4.6 \times 10^{33} \text{ cm}^{-2} \text{ s}^{-1}. \quad (6)$$

In the case of the $\mu^+\mu^+$ collider, both of the beams reduce their intensities due to the muon decay. For the operation at 50 Hz, the time averaged reduction due to the decay is $(1 - 1/e^2)/2$ rather than $(1 - 1/e)^2$. Noting this, we obtain the luminosity of the $\mu^+\mu^+$ collider as

$$\mathcal{L}_{\mu^+\mu^+} = 5.7 \times 10^{32} \text{ cm}^{-2} \text{ s}^{-1}. \quad (7)$$

These luminosities in Eqs. (6) and (7) are delivered for each detector if we have multiple collision points in the storage ring.

Although the precise numbers depend on the various efficiencies for the muon production as well as the detail designs of the muon accelerator and the storage ring, the above estimates represent the realistic orders of magnitudes that one can achieve with currently available technologies. Detail studies of each component are desired for more precise estimates.

2.5 Large ring option

It is possible to consider the option to have a larger storage ring with a higher energy. For example, one can consider a 3 TeV muon beam with the storage ring with the circumference of 9 km. In this case, due to the longer muon lifetime, the muons can travel larger distances while a larger ring reduces the collision frequency by 1/3. The luminosities are, however, kept unchanged since this reduction of the collision frequency can be compensated by the

improved beam emittance due to the higher energy. In addition, the acceleration to the higher energy actually requires the same electric power at the booster ring (9 MW) since the repetition rate can be reduced by the same factor due to the longer lifetime. In total, there is no much gain in terms of luminosities by going to higher energies unless we increase the beam power.

2.6 Beam polarizations

The design of the muon $g-2$ experiment at J-PARC aims at the polarization of $P_{\mu^+} > 0.9$ [14]. The surface muons produced by the decay of π^+ are 100 % polarized due to the $V - A$ structure of the weak interaction. Under the magnetic field of order 0.3 T in the longitudinal direction, the spin of μ^+ is maintained in the formation of the muonium, and a highly polarized muon beam can be extracted after the laser ionization. Although the understanding of the disturbance of the beam emittance by the magnetic field seems to require more study, we assume in this work that $P_{\mu^+} = 0.8$ can be obtained. At worst, without the longitudinal magnetic field, the formation of the muonium still leaves the 50 % polarization at each muonium production as the $| + + \rangle$ muonium states maintains the muon spin while $| + - \rangle$ states undergo the spin oscillation. The muonium productions at two targets would reduce the polarization to $P_{\mu^+} = 0.5^2 = 0.25$. The difference between $P_{\mu^+} = 0.8$ and 0.25 at μ^+e^- colliders results in 30 % decrease in the cross sections of the WW fusion process for the Higgs boson production. In the case of the $\mu^+\mu^+$ collider, the cross sections of purely left-handed muon process, such as the productions of supersymmetric particles discussed below, will be reduced by a factor of two.

The beam polarization option of the e^- beam at the SuperKEKB experiment has been studied [13]. The polarized electron source and spin rotators placed right before and after the interaction region(s) have been considered, with the targeted polarization of $P_{e^-} = \pm 0.7$. We assume that the same technology can be implemented in the μ^+e^- colliders.

2.7 Magnet design

As the reference design, we assumed the circumference of the storage ring as the size of the TRISTAN ring, 3 km. The electron energy of 30 GeV is the maximum energy reached in the TRISTAN experiments. For steering of the 1 TeV muon beam within the 3 km ring, we need a dipole magnet with the magnetic field of 10 T, which is a similar strength as the design of the high-luminosity LHC experiments of 11 T. The prototypes of utilizing the

Nb₃Sn superconducting technologies have already been produced and tested [17].

If we assume that a larger magnetic field such as 16 T is available by then, a smaller storage ring is possible. For example, the large ring option of the 9 km circumference can be reduced to about 6 km although we still need a large booster ring for the acceleration. The reduced one can certainly fit realistic experimental sites such as at the Tevatron site (μ Tevatron).

3 Higgs boson production at μ TRISTAN

Based on the estimated luminosity in the previous section, we discuss the rate of the Higgs boson production at the μ^+e^- collider with the energies $(E_{e^-}, E_{\mu^+}) = (30 \text{ GeV}, 1 \text{ TeV})$. We assume that the beam polarizations with $P_{e^-} = \pm 0.7$ and $P_{\mu^+} = \pm 0.8$ are possible. We set the polarizations to be $(P_{e^-}, P_{\mu^+}) = (-0.7, 0.8)$, which maximizes the cross section of the W boson fusion process.

Using these parameters, the cross sections of the single Higgs boson production via the W boson fusion (WBF) and the Z boson fusion (ZBF) processes, respectively, are given by

$$\sigma_{\text{WBF}} \approx 91 \text{ fb}, \quad \sigma_{\text{ZBF}} \approx 4 \text{ fb}. \quad (8)$$

These cross sections and the energy and angular distributions of the Higgs boson productions discussed below are all those at the parton level, and they are calculated by using the MadGraph5 [18].

The integrated luminosity of 1 ab^{-1} can be achieved by ten years of running by assuming the duty factor of 70 % and a single detector. With this integrated luminosity, the number of Higgs boson events is then estimated to be

$$N(\text{Higgs}) = 9.5 \times 10^4 \times \left(\frac{\text{integrated luminosity}}{1.0 \text{ ab}^{-1}} \right). \quad (9)$$

This huge number of Higgs events can be used for the precise measurements of the Higgs boson couplings. In the κ scheme, where κ parameters are multiplied to the Standard Model couplings, the number of the Higgs production via WBF followed by the $H \rightarrow b\bar{b}$ decay is proportional to $\kappa_W^2 \kappa_b^2 / \kappa_H^2$, where κ_W and κ_b are the Higgs boson coupling to the W boson and the b quark normalized by the Standard Model values. κ_H is defined as $\Gamma_H = \kappa_H^2 \Gamma_H^{\text{SM}}$, where Γ_H denotes the total decay width of the Higgs boson. Comparing this prediction with the experimental data, one can restrict the deviations from unity. The statistical uncertainties

for the deviation is estimated to be

$$\begin{aligned} \Delta(\kappa_W + \kappa_b - \kappa_H)_{\text{stat}} &= \frac{1}{2} \frac{1}{\sqrt{N(\text{WBF}) \times \text{Br}(h \rightarrow b\bar{b}) \times \text{efficiency}}} \\ &= 3.1 \times 10^{-3} \times \left(\frac{\text{integrated luminosity}}{1.0 \text{ ab}^{-1}} \right)^{-1/2} \left(\frac{\text{efficiency}}{0.5} \right)^{-1/2}. \end{aligned} \quad (10)$$

Here the branching ratio, $\text{Br}(h \rightarrow b\bar{b}) = 5.82 \times 10^{-1}$, is used, and it is assumed that the number of the background events gets much less than that of the signal events by appropriate selection cuts. The efficiency is assumed to be 50%, which actually depends on the energy resolutions and event selections. As a reference, in Ref. [19] the event selections at the ILC at $\sqrt{s} = 250$ GeV and 500 GeV are considered, which gives the efficiencies of order 15% and 40%, respectively. In the μ^+e^- colliders, there are no processes with the final state W^+W^- , ZZ , $q\bar{q}$ or Zh , which significantly contribute to background events, and thus the event selection would be able to be much looser.

The main background is the Z boson production followed by the decay into bottom quark pair, $e^- \mu^+ \rightarrow \nu_e \bar{\nu}_\mu Z \rightarrow \nu_e \bar{\nu}_\mu b\bar{b}$. The invariant mass of the two b jets is peaked at the Z boson mass, but give an overlap in the Higgs mass region by the finite energy resolutions of the detector. The number of the events is at the same level as those of the signals:

$$N_{\text{BG}} = 5.5 \times 10^4 \times \left(\frac{\text{integrated luminosity}}{1.0 \text{ ab}^{-1}} \right). \quad (11)$$

The selection cut on the $b\bar{b}$ invariant mass should significantly reduce this background. For example, the study in Ref. [19] have reported that 95% (90%) of the $Z \rightarrow b\bar{b}$ background events are rejected by the cut at $\sqrt{s} = 250$ GeV (500 GeV) while about 80% of the signal events survive. We therefore anticipate that the efficiency of 50%, assumed e.g. in Eq. (10), provides reasonable estimates.

The study in Ref. [10] reported the precision of the Higgs coupling to be a percent level by performing a fast detector simulation. A better sensitivity in Eq. (10) is partly due to enhanced cross sections by the beam polarization. One should, however, study the detector performance to obtain a realistic estimate. As we discuss in Section 5, the coverage and the performance in the forward region (the μ^+ direction) is especially important.

Decay modes other than $h \rightarrow b\bar{b}$ and the Higgs production via ZBF should also be able to be used for the measurements of the coupling constants and would be useful in disentangling individual couplings such as κ_W and κ_b rather than its combinations. Compared to the e^+e^- or $\mu^+\mu^-$ colliders, the domination of the WBF process for the Higgs production is a limitation for this respect, although the measurements of the subdominant ZBF processes may give an

interesting input. See Refs. [20, 21, 22] for the studies of the Higgs coupling measurements at future colliders. It is important to perform a thorough study of the performance of this collider for the Higgs coupling measurements to compare with other future colliders. We will leave such studies for future works as we need to fix the detector design to proceed. Our first estimate of the number of the Higgs events is indicating that the μ TRISTAN can potentially be an interesting realistic option for the near future.

The $\mu^+\mu^+$ collider at $\sqrt{s} = 2$ TeV can also produce the Higgs boson via the Z boson fusion process. The cross section of the Higgs production at $\sqrt{s} = 2$ TeV is estimated to be about 54 fb by assuming the polarized beam $P_{\mu^+} = 0.8$ for both of μ^+ . Although the vector boson fusion process is enhanced by a logarithmic factor, $\log s$, the small coupling between the lepton and the Z boson results in a smaller cross section than $\sigma_{\text{WBF}} + \sigma_{\text{ZBF}}$ in Eq. (8). Since the luminosity is expected to be reduced by about a factor of ten compared to μ^+e^- colliders, the precision measurements of the Higgs couplings are better performed at the low energy μ^+e^- option. Even with the reduced luminosity, the $\mu^+\mu^+$ collider has a much better capability of supersymmetry searches as we discuss later.

4 μ Tevatron option

The option with a larger storage ring, such as the size of the Tevatron (the circumference of about 6 km), can provide higher energy beams. By assuming the same luminosities, one can achieve better precision of the Higgs boson couplings. The pair production of Higgs bosons has a large cross section, which makes it possible to measure the three-point self coupling of the Higgs boson. We assume that the electron energy of 50 GeV and the muon beam energy of 3 TeV are possible by using the improved bending magnet (or having 9 km ring).

The cross section of the single Higgs boson production is enhanced as the energy increases. At $(E_{e^-}, E_{\mu^+}) = (50 \text{ GeV}, 3 \text{ TeV})$, which gives $\sqrt{s} = 775 \text{ GeV}$, the WBF and ZBF cross sections are given by

$$\sigma_{\text{WBF}} \approx 472 \text{ fb}, \quad \sigma_{\text{ZBF}} \approx 20 \text{ fb}. \quad (12)$$

The number of the Higgs boson production events is estimated as

$$N(\text{higgs}) = 4.9 \times 10^5 \times \left(\frac{\text{integrated luminosity}}{1.0 \text{ ab}^{-1}} \right), \quad (13)$$

and the precision of the κ parameters is

$$\Delta(\kappa_W + \kappa_b - \kappa_H)_{\text{stat}} = 1.3 \times 10^{-3} \times \left(\frac{\text{integrated luminosity}}{1.0 \text{ ab}^{-1}} \right)^{-1/2} \left(\frac{\text{efficiency}}{0.5} \right)^{-1/2}. \quad (14)$$

The cross section of the Higgs boson pair production process $e^- \mu^+ \rightarrow \nu_e \bar{\nu}_\mu hh$ is given by

$$\sigma \approx 8.9 \times 10^{-2} \text{ fb.} \quad (15)$$

We find the number of events to be

$$N(\text{Higgs pair}) = 89 \times \left(\frac{\text{integrated luminosity}}{1.0 \text{ ab}^{-1}} \right). \quad (16)$$

With this number, one should be able to measure the three-point coupling at the level of ten to a hundred percent.

The good precision of the single Higgs production in Eq. (14) is already sensitive to the radiative corrections to the Higgs coupling [23]. The effects of the three-point Higgs coupling to the WBF process at the one-loop level is found to be $0.006\kappa_\lambda$ [24], where κ_λ is the three point coupling normalized by the Standard Model prediction. This means that the measurement of $\Delta\kappa_\lambda$ of $\mathcal{O}(20\%)$ is already possible with the single Higgs production measurements.

5 Asymmetric μ^+e^- colliders and detector design

The asymmetry in the energies of the colliding beams, 30 GeV and 1 TeV, or 50 GeV and 3 TeV, makes the final state particles to be boosted to the direction of the μ^+ beam. The detector should be designed such that the small-angle region from the beam direction is covered.

The boost factors from the center-of-mass frame are $\gamma = 3.0$ and 3.9 , respectively, for the Higgs boson produced at colliders with energies (30 GeV, 1 TeV) and (50 GeV, 3 TeV). This makes the typical polar angle of the final state particles to be a few to ten degrees in the lab frame. In Fig. 3, we show distribution of the polar angle and the momentum of the Higgs boson produced by the WW fusion process. We see that the distribution is peaked at $\theta \sim 5 - 10$ degrees. The b and \bar{b} quarks from the decay of the Higgs bosons have the distributions shown in Fig. 4. The fraction of the events where both b and \bar{b} are in the direction of $\theta > \theta_{\text{cut}}$, is shown in Fig. 5. In order to accept significant fractions of the events, we need a good detector coverage in the forward direction, such as below a few degrees. This requirement may be a challenge in designing detectors, but it should not be too severe by comparing with the coverage of the forward region in the LHCb detector ($\theta > 15$ mrad) [25] or those of the designs of the electron-proton [26] and electron-ion colliders [27].

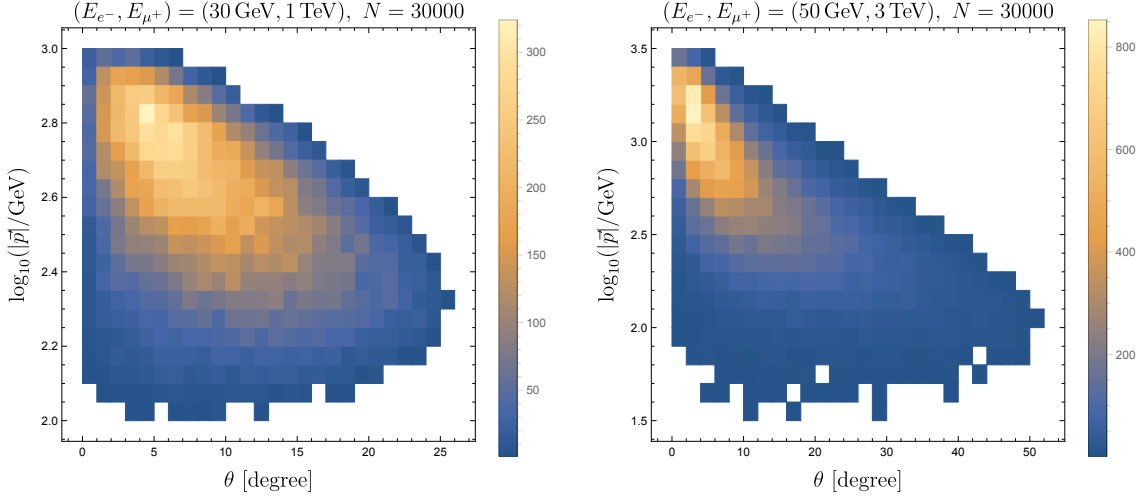


Figure 3: Density histogram plots of Higgs boson produced by the W -fusion. The number of the event is $N = 30000$. The vertical and horizontal axes represent the 3D momentum and angle from the beam axis, respectively. (Left): The beam energy is $(E_{e^-}, E_{\mu^+}) = (30 \text{ GeV}, 1 \text{ TeV})$. (Right): The beam energy is $(E_{e^-}, E_{\mu^+}) = (50 \text{ GeV}, 3 \text{ TeV})$.

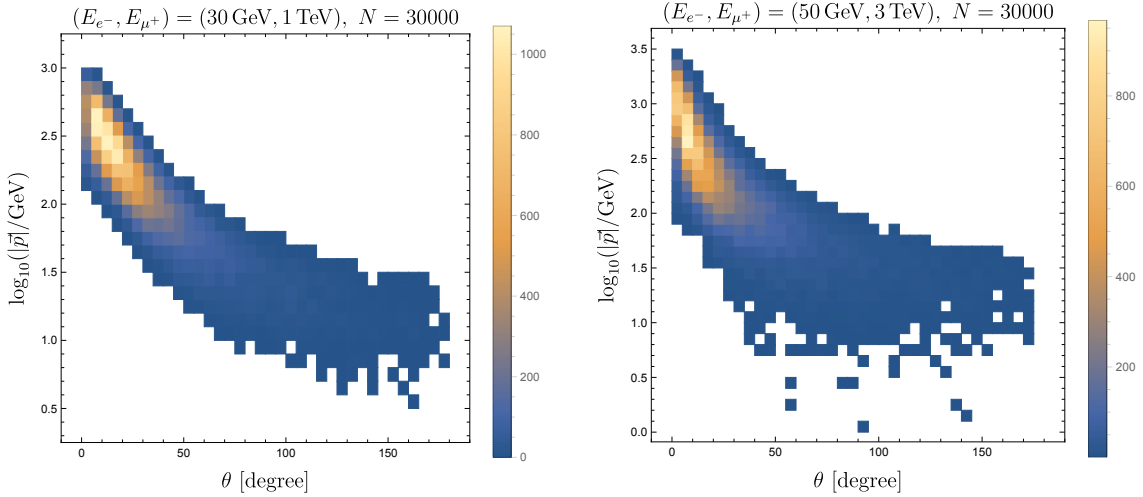


Figure 4: Density histogram plots of b quark produced by the decay channel $h \rightarrow b\bar{b}$. The number of the event is $N = 30000$. The vertical and horizontal axes represent the 3D momentum and angle from the beam axis, respectively. (Left): The beam energy is $(E_{e^-}, E_{\mu^+}) = (30 \text{ GeV}, 1 \text{ TeV})$. The distribution peaks around $|\vec{p}| \simeq 316 \text{ GeV}$ and $\theta \simeq 10^\circ$. (Right): The beam energy is $(E_{e^-}, E_{\mu^+}) = (50 \text{ GeV}, 3 \text{ TeV})$. The distribution peaks around $|\vec{p}| \simeq 500 \text{ GeV}$ and $\theta \simeq 7.5^\circ$.

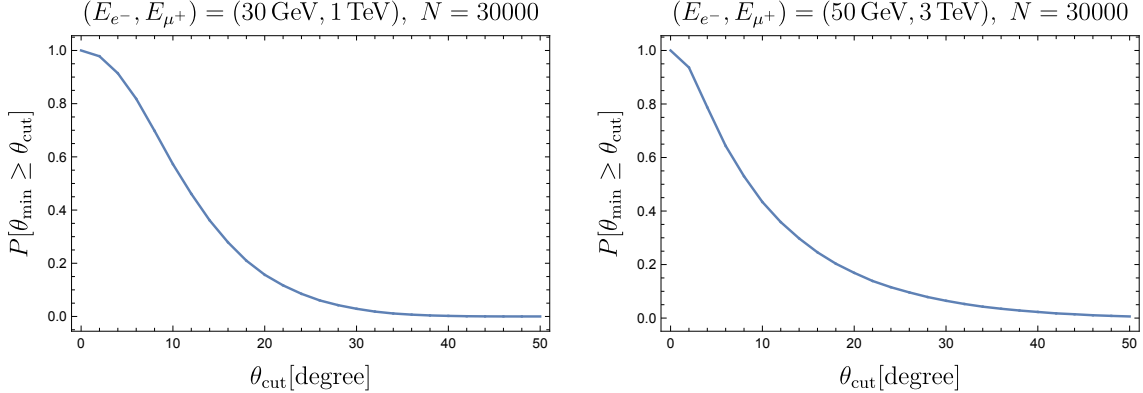


Figure 5: Plots for the number distribution of events such that $\theta_{\min} \equiv \min\{\theta_b, \theta_{\bar{b}}\}$ satisfies $\theta_{\min} \geq \theta_{\text{cut}}$. They are normalized by the number of the entire events, $N = 30000$. (Left): The beam energy is $(E_{e^-}, E_{\mu^+}) = (30 \text{ GeV}, 1 \text{ TeV})$. (Right): The beam energy is $(E_{e^-}, E_{\mu^+}) = (50 \text{ GeV}, 3 \text{ TeV})$. In both cases, one needs θ_{cut} to be less than a few degree for detecting 90 % of $h \rightarrow b\bar{b}$ events.

In the design of detectors, one should also take into account the background from the decay products of the beam muons [6]. One should shield the interaction region from the positrons and photons in the μ^+ beam, and should also have good efficiency to reject unwanted tracks. Although placing a shield from the μ^+ beam reduces the η coverage in the direction of the e^- beam, physics performance would not be significantly affected since the asymmetry in the beam energies makes the most of the physics events boosted in the μ^+ direction as we discussed above. In any case, dedicated studies on the detector designs are necessary to discuss the physics performance of the μ^+e^- colliders.

6 Superparticle searches at μ^+e^- and $\mu^+\mu^+$ colliders

The μ^+e^- and also $\mu^+\mu^+$ colliders have a capability of producing new particles if kinematically accessible. As an example, we demonstrate the case with supersymmetry where scalar leptons are produced through the diagrams of the exchange of $SU(2)_L$ gauginos, the Winos. For simplicity, we ignore the Bino (the partner of $U(1)_Y$ gauge boson) and the Higgsino contributions, and we do not consider decays of the scalar leptons, and just count the number of production events with luminosities estimated in Section 2. In the case where the lightest superparticle is one of the neutralinos, the final states are $e^-\mu^+$ and missing energy. The threshold scan of the collider energy (and/or the polarization dependence of the event rate) should be able to detect the signal if the number of the events is large enough. We will demonstrate the reaches by requiring $O(100)$ events per year. In the actual model, for

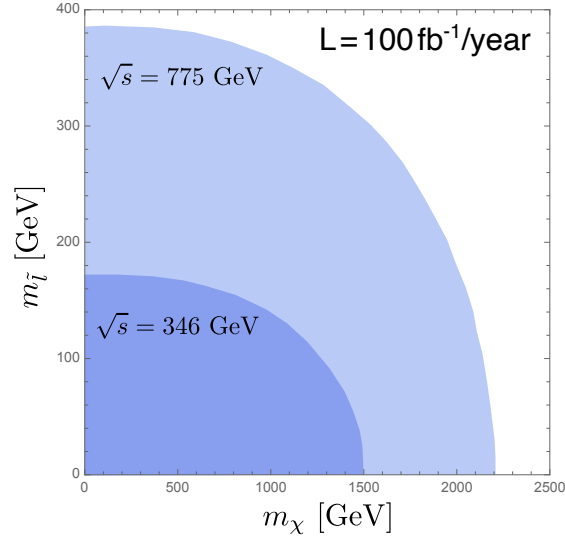


Figure 6: The region where the number of the charged slepton pair production per year is larger than a hundred at the μ^+e^- collider. We take the luminosity to be $\mathcal{L} = 100 \text{ fb}^{-1}/\text{year}$. The beam polarizations are taken to be $P_{e^-} = -0.7$ and $P_{\mu^+} = 0.8$. The scalar lepton masses are taken to be the same, $m_{\tilde{l}} = m_{\tilde{e}} = m_{\tilde{\mu}}$.

example, in the case of the Bino as the lightest supersymmetric particle, one should also include the production process through the exchange of the Bino. Since the discussion will be complicated when we include all the supersymmetric particles, we ignore those amplitudes for simplicity.

The LHC experiments have searched for the events of the pair production of the scalar leptons, and have excluded the region of the scalar lepton masses less than about 700 GeV [28, 29] when the mass difference between the scalar lepton and the lightest neutralino is larger than about 100 GeV. The center of mass energy of the μ^+e^- collider, $\sqrt{s} = 346$ GeV or 775 GeV, would not allow to go beyond the LHC limits in terms of the scalar lepton masses. It may, however, cover the region of the smaller mass differences. The $\mu^+\mu^+$ colliders, on the other hand, can reach TeV scale scalar leptons directly as we discuss below.

6.1 $e^- + \mu^+ \rightarrow \tilde{e}^- + \tilde{\mu}^+$

At the μ^+e^- colliders, the diagram with neutralino exchange gives the production of a scalar electron and a scalar muon. The differential cross section can be obtained as

$$d\sigma = \frac{d\cos\theta}{32\pi} \frac{(1+x_3-x_4)\beta}{s} |M_{\text{LR}}|^2 \frac{(1-P_{e^-})(1+P_{\mu^+})}{4}, \quad -1 \leq \cos\theta \leq 1, \quad (17)$$

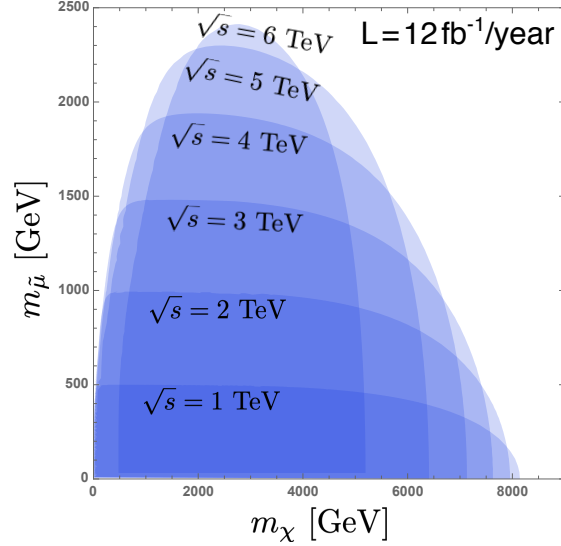


Figure 7: The region where the number of the charged slepton pair production per year is larger than a hundred at the $\mu^+\mu^+$ collider. We take the luminosity to be $\mathcal{L} = 12 \text{ fb}^{-1}/\text{year}$. The beam polarizations are taken to be $P_{\mu^+} = 0.8$ for both μ^+ beams.

where

$$M_{\text{LR}} = -\frac{g_2^2}{2} \cdot \frac{(1 + x_3 - x_4)\beta \sin \theta}{1 + 2x_A - x_3 - x_4 - (1 + x_3 - x_4)\beta \cos \theta}, \quad (18)$$

and

$$x_A = \frac{m_\chi^2}{s}, \quad x_3 = \frac{m_{\tilde{e}}^2}{s}, \quad x_4 = \frac{m_{\tilde{\mu}}^2}{s}, \quad \beta = \frac{\sqrt{1 - 2x_3 - 2x_4 + (x_3 - x_4)^2}}{1 + x_3 - x_4}. \quad (19)$$

The masses, m_χ , $m_{\tilde{e}}$ and $m_{\tilde{\mu}}$ are those of the neutralino, the scalar electron and the scalar muon, respectively. The coupling constant g_2 is that of the $SU(2)_L$ gauge interaction. A similar (a factor of four larger) cross section is obtained for scalar neutrino productions.

By setting the maximal optimization of the polarizations, $P_{e^-} = -0.7$ and $P_{\mu^+} = 0.8$ and assuming the yearly luminosity of 100 fb^{-1} (corresponding to the 70 % duty factor with Eq. (6)), we show in Fig. 6 the parameter region where the number of the production events is over one hundred per year. In the figure, we take the scalar electron and the scalar muon to be the same mass, $m_{\tilde{l}} = m_{\tilde{e}} = m_{\tilde{\mu}}$.

6.2 $\mu^+ + \mu^+ \rightarrow \tilde{\mu}^+ + \tilde{\mu}^+$

At the $\mu^+\mu^+$ collider, the kinematic reach of the scalar lepton production is higher while the possible luminosity is reduced in the current technology. At this collider, the neutralino

exchange provides a pair production of the scalar muons while scalar neutrino productions are forbidden by charge conservation. The process of the scalar lepton production at the same sign muon collider has been studied in Ref. [15]. A similar process at e^-e^- colliders has also been considered in Refs. [30, 31]. Non-vanishing amplitude requires the intermediate neutralino in the t and u -channel to be a Majorana fermion, and thus the amplitude is proportional to the gaugino mass. The differential cross sections is given by

$$d\sigma = \frac{d\cos\theta}{32\pi} \frac{\beta}{s} |M_{\text{RR}}|^2 \frac{(1+P_{\mu 1})(1+P_{\mu 2})}{4}, \quad 0 \leq \cos\theta \leq 1, \quad (20)$$

where

$$M_{\text{RR}} = -\frac{g_2^2}{2} \cdot \frac{4\sqrt{x_A}(1+2x_A-2x_3)}{(1+2x_A-2x_3)^2 - \beta^2 \cos^2\theta}, \quad (21)$$

and

$$x_A = \frac{m_\chi^2}{s}, \quad x_3 = \frac{m_{\tilde{\mu}}^2}{s}, \quad \beta = \sqrt{1-4x_3}. \quad (22)$$

The production angle θ can be integrated to give the total cross section as

$$\begin{aligned} \sigma = & \frac{g_2^4}{64\pi} \frac{1}{s} \left[\frac{\beta x_A}{x_A + (x_A - x_3)^2} + \frac{2x_A}{1+2x_A-2x_3} \log \frac{1+2x_A-2x_3+\beta}{1+2x_A-2x_3-\beta} \right] \\ & \times \frac{(1+P_{\mu 1})(1+P_{\mu 2})}{4}. \end{aligned} \quad (23)$$

We show in Fig. 7 the number of events per year by assuming the luminosity, $\mathcal{L} = 12 \text{ fb}^{-1} \text{ year}^{-1}$, which corresponds to 70 % of running with Eq. (7). Even with very heavy gauginos, such as 5 TeV, the yearly production rate can easily be over a hundred. Although the luminosity is lower compared to the μ^+e^- colliders, the reach is much better. This can be understood by the different \sqrt{s} dependence of the cross section. For $m_\chi \gtrsim \sqrt{s}$, one can integrate out the gaugino, and we obtain effective contact interactions. The $(\tilde{\mu}\gamma_\mu e)(\tilde{e}^*\partial^\mu\tilde{\mu})$ term for the $\tilde{e}^-\tilde{\mu}^+$ production has mass dimension of six, whereas the $\tilde{\mu}^+\tilde{\mu}^+$ production occurs through the $(\tilde{\mu}\mu^c)(\tilde{\mu}\tilde{\mu})$ term, whose mass dimension is five. This makes the $\tilde{\mu}^+\tilde{\mu}^+$ productions less suppressed for large gaugino masses. On the other hand, since the amplitude vanishes when the gaugino mass goes to zero, the small gaugino mass region is not fully covered. One can see that for $\sqrt{s} = 6 \text{ TeV}$ the reach starts to shrink for a fixed luminosity.

The searches should cover interesting parameter regions motivated by the muon $g-2$ anomaly [32, 33]. In order to explain the discrepancy between the Standard Model predictions and the experiments by the contributions from the superparticles, their masses need to be less than about TeV. For a recent study, see Ref. [34].

7 Summary

The muon collider is not just one of the options in future collider experiments. It would be the only option of energy frontier in the future as the electron or proton accelerations will soon reach the limit in terms of the size of the experiments. The muon colliders should in principle be possible, and if it realizes, physics impact is quite strong. In addition to direct reach to $O(10)$ TeV energies, they simultaneously provide good precision physics such as the Higgs boson couplings. Not only collider physics, rich muon and neutrino physics programs will be possible at the facility of the muon collider. Fortunately, we do have a technology of handling μ^+ already to form accelerator beams. This means that μ^+e^- and $\mu^+\mu^+$ colliders are realistic options at the present time and worth considering and planning seriously.

We estimated the luminosity of the μ^+e^- and $\mu^+\mu^+$ colliders with realistic accelerator parameters, and demonstrated that the μ^+e^- colliders serve as very good Higgs boson factories. For the $\mu^+\mu^+$ colliders, the luminosity is reduced in the current technology. Nevertheless, it is already found to be good enough to search for new particles such as superparticles.

There are numbers of works to be done. One should consider the design of the detectors and study physics capabilities based on it. The measurements of the Higgs boson couplings can be done by using decay modes other than $h \rightarrow b\bar{b}$ such as $h \rightarrow WW^*$, $\tau^+\tau^-$, and ZZ^* . Various new physics models other than supersymmetry can be searched at μ^+e^- and $\mu^+\mu^+$ colliders. The option of $\gamma\mu^+$ colliders may also be interesting to explore since that would directly prove the microscopic physics to explain the muon $g - 2$ anomaly.

The problem of the neutrino radiations from the muon decay in the beam also needs to be seriously considered [35]. Although the problem is less severe than 10 TeV class muon colliders, going into deep underground and/or a careful design of the beam transportation such as a tilt in the accelerating and interaction regions may be needed.

Acknowledgements

We would like to thank Takayuki Yamazaki, Cedric Zhang, and Shusei Kamioka for providing us with information of the muon yields on which our estimates are based. The work is supported by JSPS KAKENHI Grant Nos. JP19H00689 (RK, RM), JP19K14711 (HT), JP21H01086 (RK), JP21J01117 (YH) and MEXT KAKENHI Grant No. JP18H05542 (RK, HT).

References

- [1] *The International Linear Collider Technical Design Report - Volume 1: Executive Summary*, 6 2013, [arXiv:1306.6327 \[physics.acc-ph\]](#).
- [2] T. K. Charles *et al.*, *The Compact Linear Collider (CLIC) - 2018 Summary Report*, vol. 2/2018, 12 2018, [doi:10.23731/CYRM-2018-002](#), [arXiv:1812.06018 \[physics.acc-ph\]](#).
- [3] J. C. Gallardo *et al.*, $\mu^+\mu^-$ Collider: Feasibility Study, *eConf*, vol. C960625, p. R4, 1996.
- [4] C. M. Ankenbrandt *et al.*, *Status of muon collider research and development and future plans*, *Phys. Rev. ST Accel. Beams*, vol. 2, p. 081001, 1999, [doi:10.1103/PhysRevSTAB.2.081001](#), [arXiv:physics/9901022](#).
- [5] H. Al Ali *et al.*, *The Muon Smasher's Guide*, 3 2021, [arXiv:2103.14043 \[hep-ph\]](#).
- [6] N. Bartosik *et al.*, *Detector and Physics Performance at a Muon Collider*, *JINST*, vol. 15, no. 05, p. P05001, 2020, [doi:10.1088/1748-0221/15/05/P05001](#), [arXiv:2001.04431 \[hep-ex\]](#).
- [7] T. Han, D. Liu, I. Low, and X. Wang, *Electroweak couplings of the Higgs boson at a multi-TeV muon collider*, *Phys. Rev. D*, vol. 103, no. 1, p. 013002, 2021, [doi:10.1103/PhysRevD.103.013002](#), [arXiv:2008.12204 \[hep-ph\]](#).
- [8] J. P. Delahaye, M. Diemoz, K. Long, B. Mansoulié, N. Pastrone, L. Rivkin, D. Schulte, A. Skrinsky, and A. Wulzer, *Muon Colliders*, 1 2019, [arXiv:1901.06150 \[physics.acc-ph\]](#).
- [9] Y. Kondo *et al.*, *Re-Acceleration of Ultra Cold Muon in J-PARC Muon Facility*, in *9th International Particle Accelerator Conference*, 6 2018.
- [10] M. Lu, A. M. Levin, C. Li, A. Agapitos, Q. Li, F. Meng, S. Qian, J. Xiao, and T. Yang, *The physics case for an electron-muon collider*, *Adv. High Energy Phys.*, vol. 2021, p. 6693618, 2021, [doi:10.1155/2021/6693618](#), [arXiv:2010.15144 \[hep-ph\]](#).
- [11] F. Bossi and P. Ciafaloni, *Lepton Flavor Violation at muon-electron colliders*, *JHEP*, vol. 10, p. 033, 2020, [doi:10.1007/JHEP10\(2020\)033](#), [arXiv:2003.03997 \[hep-ph\]](#).
- [12] T. Abe *et al.*, *Belle II Technical Design Report*, 11 2010, [arXiv:1011.0352 \[physics.ins-det\]](#).

- [13] M. Roney, *Upgrading SuperKEKB with polarized e- beams*, *PoS*, vol. ICHEP2020, p. 699, 2021, [doi:10.22323/1.390.0699](https://doi.org/10.22323/1.390.0699).
- [14] M. Abe *et al.*, *A New Approach for Measuring the Muon Anomalous Magnetic Moment and Electric Dipole Moment*, *PTEP*, vol. 2019, no. 5, p. 053C02, 2019, [doi:10.1093/ptep/ptz030](https://doi.org/10.1093/ptep/ptz030), [arXiv:1901.03047](https://arxiv.org/abs/1901.03047) [[physics.ins-det](#)].
- [15] C. A. Heusch and F. Cuypers, *Physics with like-sign muon beams in a TeV muon collider*, *AIP Conf. Proc.*, vol. 352, pp. 219–231, 1996, [doi:10.1063/1.49345](https://doi.org/10.1063/1.49345), [arXiv:hep-ph/9508230](https://arxiv.org/abs/hep-ph/9508230).
- [16] E. Oset, M. J. Vicente-Vacas, and C. Garcia-Recio, eds., *Pions in nuclei. Proceedings, International Workshop, Peniscola, Spain, June 3-8, 1991*, 1992.
- [17] B. Bordini, L. Bottura, A. Devred, L. Fiscarelli, M. Karppinen, G. de Rijk, L. Rossi, F. Savary, and G. Willering, *Nb₃Sn 11 T Dipole for the High Luminosity LHC (CERN)*, pp. 223–258. 2019.
- [18] J. Alwall, R. Frederix, S. Frixione, V. Hirschi, F. Maltoni, O. Mattelaer, H. S. Shao, T. Stelzer, P. Torrielli, and M. Zaro, *The automated computation of tree-level and next-to-leading order differential cross sections, and their matching to parton shower simulations*, *JHEP*, vol. 07, p. 079, 2014, [doi:10.1007/JHEP07\(2014\)079](https://doi.org/10.1007/JHEP07(2014)079), [arXiv:1405.0301](https://arxiv.org/abs/1405.0301) [[hep-ph](#)].
- [19] C. Dürig, K. Fujii, J. List, and J. Tian, *Model Independent Determination of HWW coupling and Higgs total width at ILC*, in *International Workshop on Future Linear Colliders*, 3 2014, [arXiv:1403.7734](https://arxiv.org/abs/1403.7734) [[hep-ex](#)].
- [20] H. Abramowicz *et al.*, *Higgs physics at the CLIC electron–positron linear collider*, *Eur. Phys. J. C*, vol. 77, no. 7, p. 475, 2017, [doi:10.1140/epjc/s10052-017-4968-5](https://doi.org/10.1140/epjc/s10052-017-4968-5), [arXiv:1608.07538](https://arxiv.org/abs/1608.07538) [[hep-ex](#)].
- [21] P. Bambade *et al.*, *The International Linear Collider: A Global Project*, 3 2019, [arXiv:1903.01629](https://arxiv.org/abs/1903.01629) [[hep-ex](#)].
- [22] J. de Blas *et al.*, *Higgs Boson Studies at Future Particle Colliders*, *JHEP*, vol. 01, p. 139, 2020”, [doi:10.1007/JHEP01\(2020\)139](https://doi.org/10.1007/JHEP01(2020)139), [arXiv:1905.03764](https://arxiv.org/abs/1905.03764) [[hep-ph](#)].
- [23] M. McCullough, *An Indirect Model-Dependent Probe of the Higgs Self-Coupling*, *Phys. Rev. D*, vol. 90, no. 1, p. 015001, 2014, [doi:10.1103/PhysRevD.90.015001](https://doi.org/10.1103/PhysRevD.90.015001), [arXiv:1312.3322](https://arxiv.org/abs/1312.3322) [[hep-ph](#)]. [Erratum: *Phys.Rev.D* 92, 039903 (2015)].

- [24] S. Di Vita, G. Durieux, C. Grojean, J. Gu, Z. Liu, G. Panico, M. Riembau, and T. Vantalón, *A global view on the Higgs self-coupling at lepton colliders*, *JHEP*, vol. 02, p. 178, 2018, doi:10.1007/JHEP02(2018)178, arXiv:1711.03978 [hep-ph].
- [25] A. A. Alves, Jr. *et al.*, *The LHCb Detector at the LHC*, *JINST*, vol. 3, p. S08005, 2008, doi:10.1088/1748-0221/3/08/S08005.
- [26] P. Agostini *et al.*, *The Large Hadron-Electron Collider at the HL-LHC*, 7 2020, arXiv:2007.14491 [hep-ex].
- [27] A. Accardi *et al.*, *Electron Ion Collider: The Next QCD Frontier: Understanding the glue that binds us all*, *Eur. Phys. J. A*, vol. 52, no. 9, p. 268, 2016, doi:10.1140/epja/i2016-16268-9, arXiv:1212.1701 [nucl-ex].
- [28] G. Aad *et al.*, *Search for electroweak production of charginos and sleptons decaying into final states with two leptons and missing transverse momentum in $\sqrt{s} = 13$ TeV pp collisions using the ATLAS detector*, *Eur. Phys. J. C*, vol. 80, no. 2, p. 123, 2020, doi:10.1140/epjc/s10052-019-7594-6, arXiv:1908.08215 [hep-ex].
- [29] A. M. Sirunyan *et al.*, *Search for supersymmetry in final states with two oppositely charged same-flavor leptons and missing transverse momentum in proton-proton collisions at $\sqrt{s} = 13$ TeV*, *JHEP*, vol. 04, p. 123, 2021, doi:10.1007/JHEP04(2021)123, arXiv:2012.08600 [hep-ex].
- [30] W.-Y. Keung and L. Littenberg, *Test of Supersymmetry in e^-e^- Collision*, *Phys. Rev. D*, vol. 28, p. 1067, 1983, doi:10.1103/PhysRevD.28.1067.
- [31] F. Cuypers, G. J. van Oldenborgh, and R. Ruckl, *Supersymmetric signals in e^-e^- collisions*, *Nucl. Phys. B*, vol. 409, pp. 128–143, 1993, doi:10.1016/0550-3213(93)90449-Y, arXiv:hep-ph/9305287.
- [32] G. W. Bennett *et al.*, *Final Report of the Muon E821 Anomalous Magnetic Moment Measurement at BNL*, *Phys. Rev. D*, vol. 73, p. 072003, 2006, doi:10.1103/PhysRevD.73.072003, arXiv:hep-ex/0602035.
- [33] B. Abi *et al.*, *Measurement of the Positive Muon Anomalous Magnetic Moment to 0.46 ppm*, *Phys. Rev. Lett.*, vol. 126, no. 14, p. 141801, 2021, doi:10.1103/PhysRevLett.126.141801, arXiv:2104.03281 [hep-ex].
- [34] M. Endo, K. Hamaguchi, S. Iwamoto, and T. Kitahara, *Supersymmetric Interpretation of the Muon $g - 2$ Anomaly*, 4 2021, arXiv:2104.03217 [hep-ph].

- [35] B. J. King, *Neutrino radiation challenges and proposed solutions for many TeV muon colliders*, *AIP Conf. Proc.*, vol. 530, no. 1, pp. 165–180, 2000, [doi:10.1063/1.1361675](https://doi.org/10.1063/1.1361675), [arXiv:hep-ex/0005006](https://arxiv.org/abs/hep-ex/0005006).